

THE DETERMINATION OF THE PHASE DIAGRAM FOR A DMPC/DSPC LIPID  
MIXTURE USING  $^2\text{H}$  NMR DIFFERENCE SPECTROSCOPY

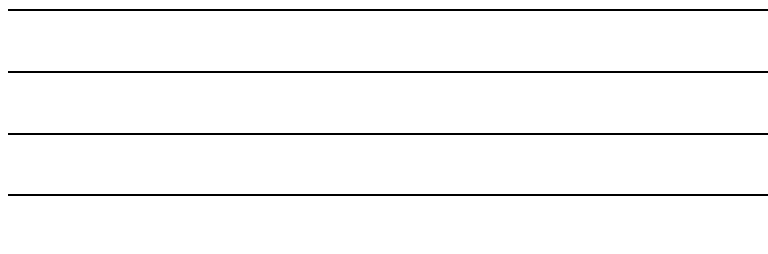
Irene Lees

A THESIS SUBMITTED IN PARTIAL FULFILLMENT OF  
THE REQUIREMENTS FOR THE DEGREE OF  
BACHELOR OF SCIENCE

in

THE FACULTY OF SCIENCE  
DEPARTMENT OF PHYSICS

We accept this thesis as conforming  
to the required standard



UNIVERSITY OF NEW BRUNSWICK

March 1991

© Irene Lees

## **Acknowledgements**

I would like to thank Dr. Sharp for being my honours project supervisor. I would especially like to thank Dr. Morrow who came up with this project and who guided me throughout the summer. I would also like to thank the other members in the NMR group at Memorial University of Newfoundland which include Alan Bell and Nestor Grandal.

This work was done with the help of an NSERC USRA.

## Table of Contents

<b>Acknowledgements</b>	<b>ii</b>
<b>List of Figures</b>	<b>v</b>
<b>List of Tables</b>	<b>vi</b>
<b>Abstract</b>	<b>vii</b>
<b>1 Introduction</b>	<b>1</b>
<b>2 Background Theory</b>	<b>3</b>
2.1 The Basics of NMR . . . . .	3
2.2 Quadrupole Echo . . . . .	12
2.3 Deuterium NMR Difference Spectroscopy . . . . .	13
<b>3 Lipids and Lipid Bilayers</b>	<b>19</b>
3.1 Lipid Structure . . . . .	19
3.2 Lipid Phases . . . . .	19
3.3 Deuterium NMR . . . . .	20
<b>4 Experimental Set-up</b>	<b>22</b>
4.1 Sample Preparation . . . . .	22
4.2 NMR Spectrometer . . . . .	23
4.3 Measurement of Quadrupole Echo . . . . .	25

<b>5</b>	<b>Results and Discussion</b>	<b>26</b>
5.1	Gel and Liquid Crystalline Spectra . . . . .	26
5.2	The Determination of the Endpoint Concentrations . . . . .	26
5.3	The Phase Diagram for DMPC/DSPC . . . . .	38
<b>6</b>	<b>Conclusion</b>	<b>42</b>
	<b>References</b>	<b>44</b>

## List of Figures

2.1	Energy levels of the spin 1 deuteron . . . . .	5
2.2	A typical “powder pattern” spectrum . . . . .	7
2.3	Tipping of the magnetization due to the application of an rf pulse . . . . .	10
2.4	A free induction decay (FID) signal. . . . .	11
2.5	Quadrupolar echo pulse sequence . . . . .	14
2.6	A phase diagram demonstrating endpoint concentrations . . . . .	16
4.1	Schematic diagram for the NMR spectrometer . . . . .	24
5.1	The characteristic spectra for the gel and liquid crystalline phases . . . . .	27
5.2	The temperature dependence of the spectra . . . . .	28
5.3	A gel endpoint subtraction . . . . .	30
5.4	A liquid crystalline endpoint subtraction . . . . .	31
5.5	The phase diagram for DMPC/DSPC . . . . .	39

## List of Tables

5.1	$R$ values . . . . .	33
5.2	$x_f$ and $x_g$ values for $R = 1$ . . . . .	36
5.3	$x_f$ and $x_g$ values for $R = 0.778$ . . . . .	37
5.4	Boundary temperatures for each concentration . . . . .	38

## Abstract

A technique called deuterium NMR difference spectroscopy was used to determine the phase diagram for a mixture of two different lipids. The two lipids studied were dimyristoylphosphatidylcholine (DMPC) and distearoylphosphatidylcholine (DSPC). Since deuterium NMR was used to acquire the data, the DMPC lipid's hydrocarbon chains were deuterated to yield DMPC<sub>d54</sub>. The lipid, at low temperatures, is in the gel phase and passes into the liquid crystalline phase as the temperature is raised. Experiments were conducted on mixtures with a variety of lipid concentrations at temperatures ranging from 4°C–50°C. The corresponding spectra obtained using <sup>2</sup>H NMR were used to calculate the endpoints of the phase boundaries at each temperature. These endpoints determined the phase diagram for the DMPC/DSPC mixture.

## Chapter 1

### Introduction

Cell membranes found in all living organisms are mainly composed of a variety of proteins and lipids. The lipids provide the structure and the proteins carry out the biological functions of the membrane.

The lipids associate to form lipid bilayers which can act as a semi-permeable barrier so that only specific molecules can enter and leave the cell. This regulation of the flow of ions and other materials into and out of the cell is crucial for the functioning and survival of the cell.

The actual cell membrane is extremely complicated and therefore very hard to study. By using much simpler models, the lipid bilayer can be investigated with known techniques which will lead us to a better understanding of the membranes found *in vivo*.

One of the simplest models that can be studied is a lipid bilayer which is formed by a mixture of only two different kinds of lipids. The two lipids used in this experiment were dimyristoylphosphatidylcholine (DMPC) and distearoylphosphatidylcholine (DSPC).

Over the years, the phase diagram for DMPC and DSPC mixtures has been studied using a variety of techniques which include differential scanning calorimetry (2,3), ESR (4), dilatometry (5) and densitometry (6). Unfortunately, no single phase diagram seems to have been accepted as the true model.

The disagreement arises from whether or not the gel phase shows miscibility (complete lipid mixing in gel phase) or immiscibility (separation of lipids into two separate gel phases) at low temperatures. There has been evidence for both sides of the argument,

depending on the technique used to determine the phase diagram.

The new method used here is called deuterium Nuclear Magnetic Resonance (NMR) difference spectroscopy (1). It can be used to determine the phases of the lipids in the lipid bilayer. This will then lead to the phase diagram, which may help solve the disagreement over the DMPC/DSPC phase diagram.

## Chapter 2

### Background Theory

#### 2.1 The Basics of NMR

The basis of Nuclear Magnetic Resonance (NMR) is that every nucleus has angular momentum  $\mathbf{I}\hbar$  and magnetic moment  $\boldsymbol{\mu} = \gamma\mathbf{I}\hbar$  associated with it, where  $\mathbf{I}$  is the angular momentum operator,  $\gamma$  is the gyromagnetic ratio and  $\hbar$  is Planck's constant divided by  $2\pi$ .

If these nuclei are placed inside a strong magnetic field,  $\mathbf{B}_0 = B_0\hat{\mathbf{k}}$ , without any electric field gradients at the nucleus, then the Hamiltonian associated with this field is given by

$$H = -\boldsymbol{\mu} \cdot \mathbf{B}_0 = -\gamma\hbar B_0 I_z \quad (2.1)$$

Since the nucleus being used in this work is the deuteron which has a spin  $I = 1$ , the Zeeman interactions split the ground state nuclear energy levels as shown in Figure 2.1a. From quantum mechanics, the eigenvalues or energy levels for the angular momentum,  $I_z$ , are

$$E_m = -\gamma\hbar B_0 m \quad (2.2)$$

where  $m = I, I - 1, \dots, -I$ . Transitions between these energy levels take place at frequencies  $\omega$  given by

$$\hbar\omega = \gamma\hbar B_0 \Delta m$$

This gives a single NMR resonance at  $\omega_0 = \gamma B_0$ .

If the sample is in thermal equilibrium at a temperature  $T$  with its surroundings (called in NMR “the lattice”) and  $\hbar\omega_0 \ll kT$ , then the population distribution of the energy levels follows Boltzmann statistics and is given by

$$\begin{aligned} p_1 &= \frac{1}{3} \left(1 + \frac{\hbar\omega_0}{kT}\right) \\ p_0 &= \frac{1}{3} \\ p_{-1} &= \frac{1}{3} \left(1 - \frac{\hbar\omega_0}{kT}\right) \end{aligned} \quad (2.3)$$

where  $P_m$  is the population of the level with quantum number  $m$ .

In addition, the deuteron has an electric quadrupole moment  $eQ$ . If there is an electric field gradient,  $eq$ , present at the nucleus, the nuclear Zeeman levels shift as in Figure 2.1b.

The nuclear quadrupole tensor is defined as

$$Q_{\alpha\beta}^N = (3x_\alpha x_\beta - \delta_{\alpha\beta} r^2) \rho \, d\tau \quad (2.4)$$

where  $\tau$  represents the nuclear volume. The electric quadrupole energy is then given by

$$E^{(2)} = 1/2 \sum_{\alpha,\beta} \nu_{\alpha\beta} Q_{\alpha\beta}^N \quad (2.5)$$

where  $\nu_{\alpha\beta} = \frac{d^2V}{dx_\alpha dx_\beta} \Big|_{r=0}$  represents the electric field gradient tensor at the nucleus.

When first order perturbation theory is used on the electric quadrupole Hamiltonian, the new energies are given by

$$E_m = \frac{e^2 q Q}{8} (3m^2 - 2) [(3\cos^2\beta - 1) + \eta \sin^2\beta \cos^2\beta] \quad (2.6)$$

This gives the levels with  $m = \pm 1$  a shift upwards by an amount

$$\Delta = \frac{e^2 q Q}{8} [(3\cos^2\beta - 1) + \eta \sin^2\beta \cos^2\alpha] \quad (2.7)$$

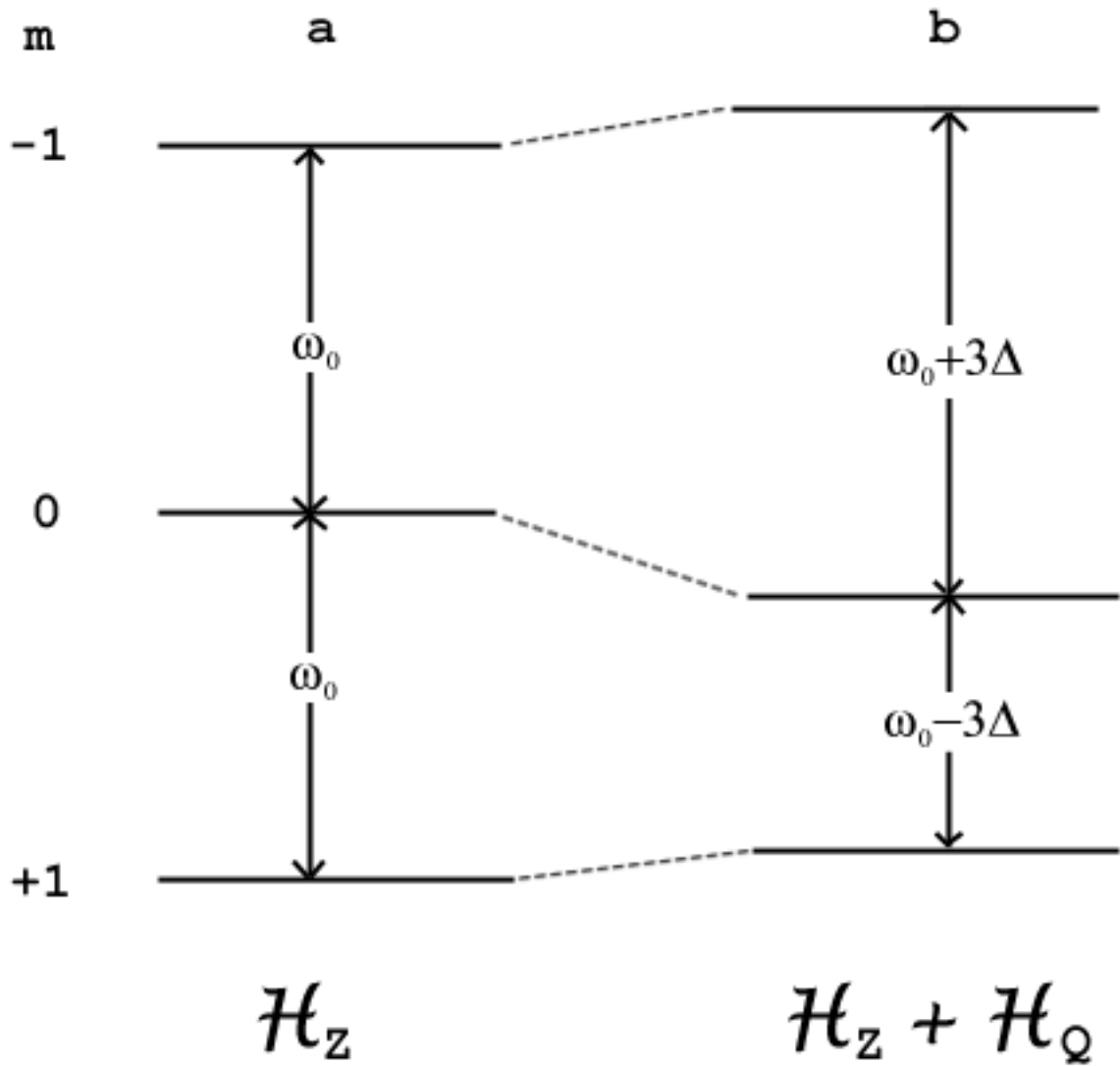


Figure 2.1: Energy levels of the spin 1 deuteron: a) splitting due to Zeeman interaction; b) first order quadrupolar shifts of the Zeeman energy levels.

and the level with  $m = 0$  a shift downwards of  $2\Delta$  (7). Therefore instead of observing a single peak at  $\omega_0$  as we do in the absence of quadrupolar interaction, we observe a doublet symmetrically placed around  $\omega_0$  with a quadrupolar splitting of

$$\omega_Q = 6\Delta = \frac{3e^2qQ}{4\hbar}[(3\cos^2\beta - 1) + \eta \sin^2\beta \cos^2\alpha] \quad (2.8)$$

where  $\eta$  is the asymmetry parameter

$$\eta = \frac{\nu_{x'x'} - \nu_{y'y'}}{\nu_{z'z'}} \quad (2.9)$$

and the angles  $\alpha$  and  $\beta$  are two of the Euler angles.

In the samples used in this work, it was not possible to orient all the molecules in the same direction. The samples have nuclei with a random distribution of orientations and the spectra are therefore called “powder pattern spectra”.

The characteristic lineshape of these spectra is found because more molecules line up perpendicularly to the magnetic field than parallel in a normal isotropic distribution. Therefore the  $90^\circ$  orientation from the static magnetic field gives the largest signal intensity represented by the large peaks and the  $0^\circ$  orientation gives the smallest signal intensity represented by the smaller shoulders, see Figure 2.2.

To induce transitions between the energy levels, a radio frequency (rf) pulse,  $B_1 \cos \omega_0 t$ , is applied at right angles to the main magnetic field (see Figure 2.3). The field  $B_1$  is much smaller than  $B_0$  so this pulse can be written as a perturbation on the Hamiltonian

$$H_{pert} = -\gamma h B_1 I_x \cos \omega_0 t \quad (2.10)$$

This magnetic field is really the superposition of two counter-rotating fields oscillating in the x-y plane. At high static magnetic fields, only the term which precesses in the same direction as the magnetizations needs to be considered.

When the frequency of  $B_1$  is near the Larmor frequency  $\omega_0$ , the nuclei in the lower levels can absorb this energy and move up to higher energy states. This causes the net

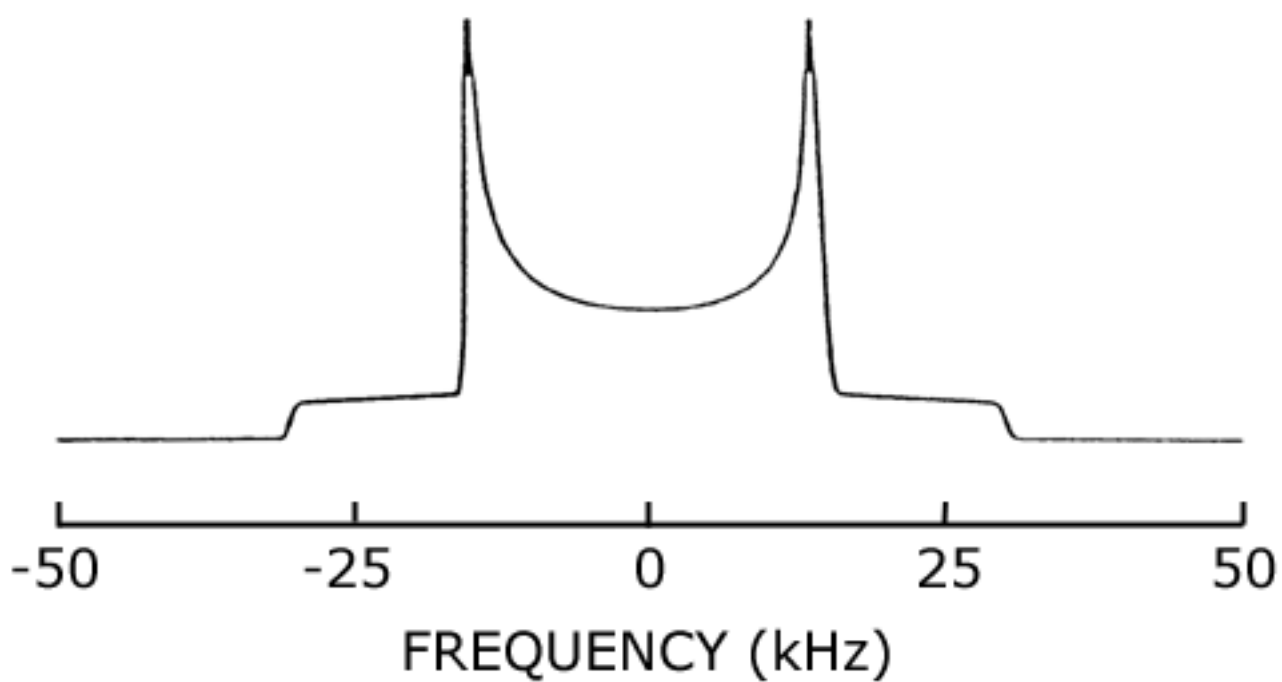


Figure 2.2: A typical “powder pattern” spectrum for spin 1 nuclei with the high peaks corresponding to nuclei with orientation perpendicular to  $\mathbf{B}_0$  and the small shoulders correspond to nuclei parallel to  $\mathbf{B}_0$ .

magnetization of the sample to tip away from its equilibrium position so that it has components  $M_x$ ,  $M_y$  and  $M_z$ .

When the rf pulse is turned off, the spins will precess around the static magnetic field at the Larmor frequency

$$\omega = -\gamma B_0 \quad (2.11)$$

where  $\gamma$  is the gyromagnetic ratio and  $B_0$  is the main magnetic field strength.

This precession will decay due to the spins redistributing their energy among themselves and the spin system relaxing back to its equilibrium population distribution. This change of the components of the magnetization has been condensed into the phenomenological Bloch equations (8)

$$\begin{aligned} \frac{dM_x}{dt} &= \gamma(M_y B_0 + M_z B_1 \sin\omega t) - \frac{M_x}{T_2} \\ \frac{dM_y}{dt} &= \gamma(M_z B_1 \cos\omega t - M_x B_0) - \frac{M_y}{T_2} \\ \frac{dM_z}{dt} &= -\gamma(M_x B_1 \sin\omega t + M_y B_1 \cos\omega t) - \frac{M_z - M_0}{T_1} \end{aligned} \quad (2.12)$$

where  $T_2$  is a characteristic time for the spins to come to internal equilibrium among themselves (spin-spin relaxation time) and  $T_1$  is the characteristic time for the spin system to relax back to its equilibrium magnetization (spin-lattice relaxation time).

Since a precessing magnetization can induce a current, a coil can be placed perpendicular to the x-y plane so that a current is induced in the coil. This allows the rate of decay of the signal to be measured, as well as the equilibrium value of the magnetization.

If we now move to a frame of reference which rotates with the motion of the magnetization then the results for the pulse sequences become much less complicated (see Figure 2.3). In this new frame, the effective magnetic field is given by

$$B_{eff} = B_0 + B_1 + \omega_0/\gamma \quad (2.13)$$

At resonance,  $\omega_0 = -\gamma B_0$  so this equation reduces to

$$B_{eff} = B_1 \quad (2.14)$$

If a pulse is applied to the sample for a duration  $t_p$  then the magnetization will precess through an angle

$$\theta = \gamma B_1 t_p \quad (2.15)$$

(see Figure 2.3). The important pulse durations for NMR experiments are those that flip the magnetization by either  $90^\circ$  or  $180^\circ$ .

There are two distinct ways in which a sample, after being perturbed by an rf pulse, relaxes back to equilibrium. To restore the longitudinal magnetization, the  $M_z$  component, to the normal +z direction, the sample releases energy to other degrees of freedom (such as vibrational, orientational, etc.) in the surrounding structure known as the lattice. For this reason, this type of relaxation is called the spin-lattice relaxation and is measured with a characteristic time constant  $T_1$ .

The other type of relaxation restores the transverse magnetization, the  $M_x$  and  $M_y$  components, by having all the spins spread out evenly in the x-y plane so that the net magnetization over all these directions is zero. This is done by the spins interacting and exchanging their energy with neighbouring nuclei so that each spin will precess at a slightly different rate. This type of relaxation is called spin-spin relaxation and is characterized by a time constant  $T_2$ .

As the spins dephase after a  $90^\circ$  pulse, the signal induced in the coil decreases with a characteristic time  $T_2$ . For this reason the signal is referred to as the free induction decay (FID). (see Figure 2.4)

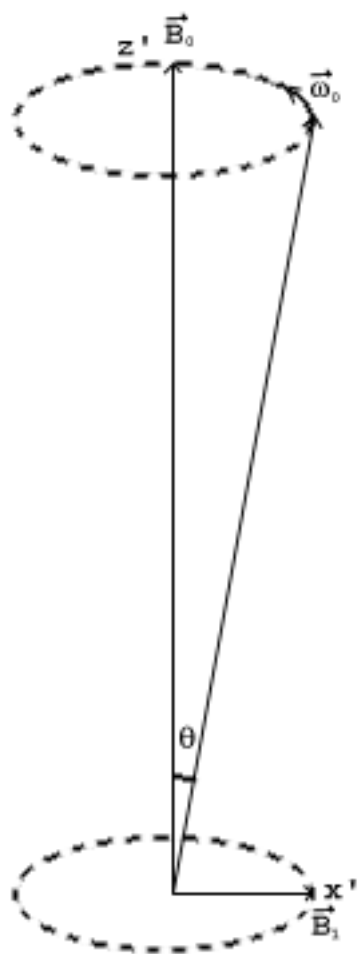


Figure 2.3: Tipping of the magnetization due to the application of an rf pulse.

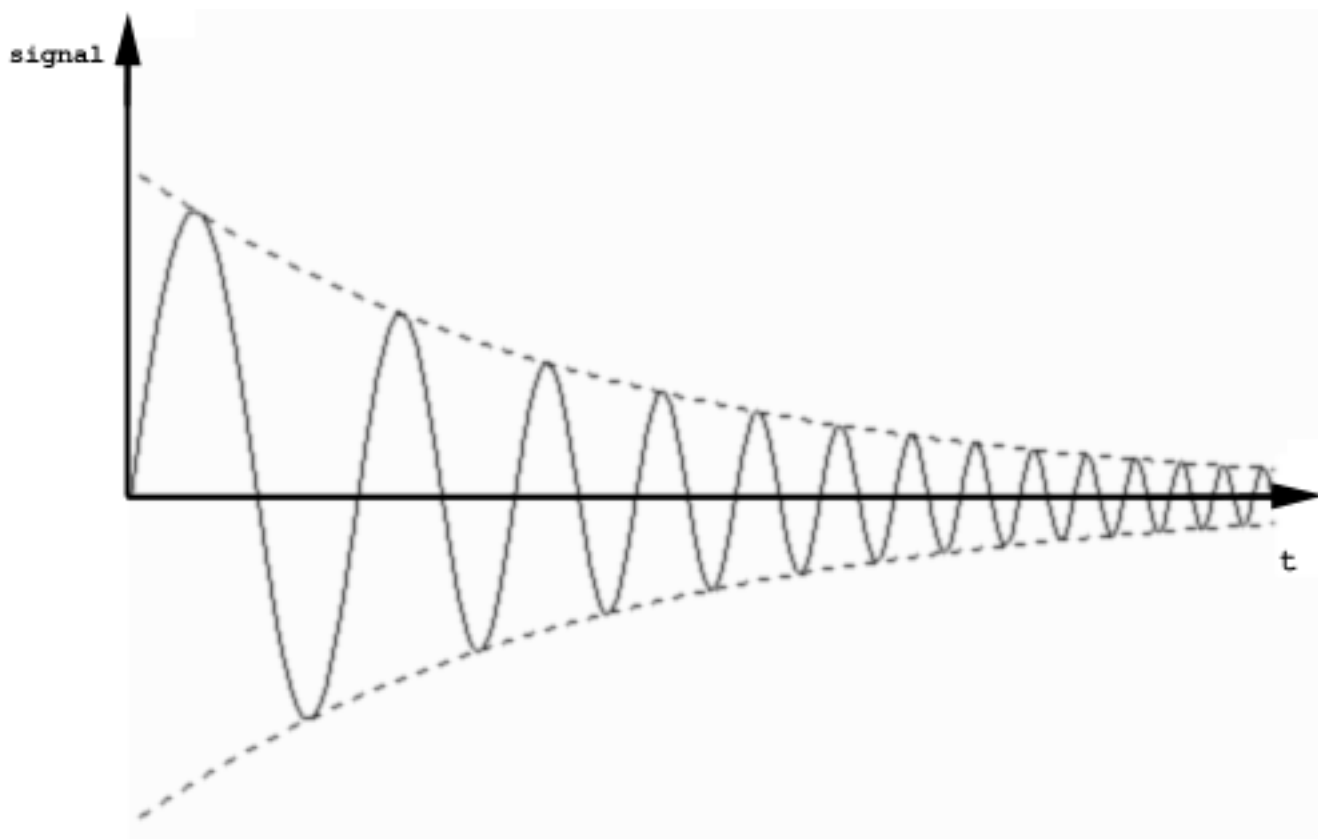


Figure 2.4: A free induction decay (FID) signal.

## 2.2 Quadrupole Echo

Over the years, several pulse sequences have been developed which help obtain information about the sample on a reasonable time scale. The classical pulse sequence is the simple free induction decay sequence consisting of an rf pulse at the approximate resonant frequency of the sample that flips the spins  $90^\circ$ . The free induction decay of the sample is measured after the pulse. The Fourier transform of this FID signal is then taken to obtain the frequency spectrum of the sample involved. This frequency spectrum can be used to determine the structure of the sample.

This technique does not work well for deuterium NMR studies because of the finite receiver dead time. When the high power pulse is applied to the sample, enough of the power leaks into the receiver to saturate it. It then takes a certain amount of time for the receiver to recover. Also, the sample coil takes a finite amount of time to stop ringing after the pulse with the amount of time depending on the  $Q$  of the coil. Only after this ringing has died down can a signal from the sample be seen. This finite amount of time is known as the receiver dead time.

For a deuteron in a C-<sup>2</sup>H bond, typical of lipid bilayers, the quadrupole splitting is about 252kHz. A free induction decay with this splitting would decay measurably during the typical receiver dead time of  $20\mu\text{s}$  and a fair bit of the signal would be lost.

A newer pulse sequence was developed that worked much better when using deuterium NMR in lipid bilayers. This pulse sequence, called the quadrupole spin echo technique, was found to enhance the signal to noise ratio and remove the problem with the spectrometer dead time (9).

This sequence starts with a  $90^\circ$  rf pulse, with a  $0^\circ$  phase shift relative to the reference phase of the receiver, that flips the sample spins into the x-y plane by causing a rotation about the x-axis. After a certain amount of time,  $\tau$ , which is greater than the receiver

dead time, a second  $90^\circ$  rf pulse, with a phase shift of  $90^\circ$  relative to the receiver reference Phase, is applied to the sample. This pulse causes a rotation about the y-axis. After another delay of time  $\tau$  the magnetization refocusses and a quadrupole spin echo is produced (see Figure 2.5).

The Fourier transform of this spectrum, starting at the top of the echo at time  $t = 2\tau$  can be used to find the order parameters which involve the direction of the C-D bonds in the hydrocarbon chains of the lipids being studied. These order parameters are a measure of the mean square amplitude of motion of the deuterons along the hydrocarbon chains of the lipid. The magnitude of this motion is directly related to the phase in which the lipid is present.

Another addition to this pulse sequence is the cycling of phases which gets rid of artifacts due to pulse imperfections and residual receiver recovery transients. This is done by varying the phase of the first pulse between  $0^\circ$  and  $180^\circ$  and second pulse between  $90^\circ$  and  $270^\circ$  relative to the receiver phase. Also, if the first pulse is applied along the y-axis instead of the x-axis and the second pulse is applied along the x-axis, then the quadrupolar echo signal is received in the channel corresponding to the x-direction (instead of the y-direction). This can be used to compare the two receiver channels.

### 2.3 Deuterium NMR Difference Spectroscopy

With the older techniques for determining the phase diagram, the phase transition of the sample was found by the deviation of the quantity being measured from a baseline. These techniques do not measure directly the phase separation of the sample. Instead they measure phase boundary, which may be affected by slight inhomogeneities in the system.

However, newer techniques like small angle neutron scattering and  $^2\text{H}$  NMR difference

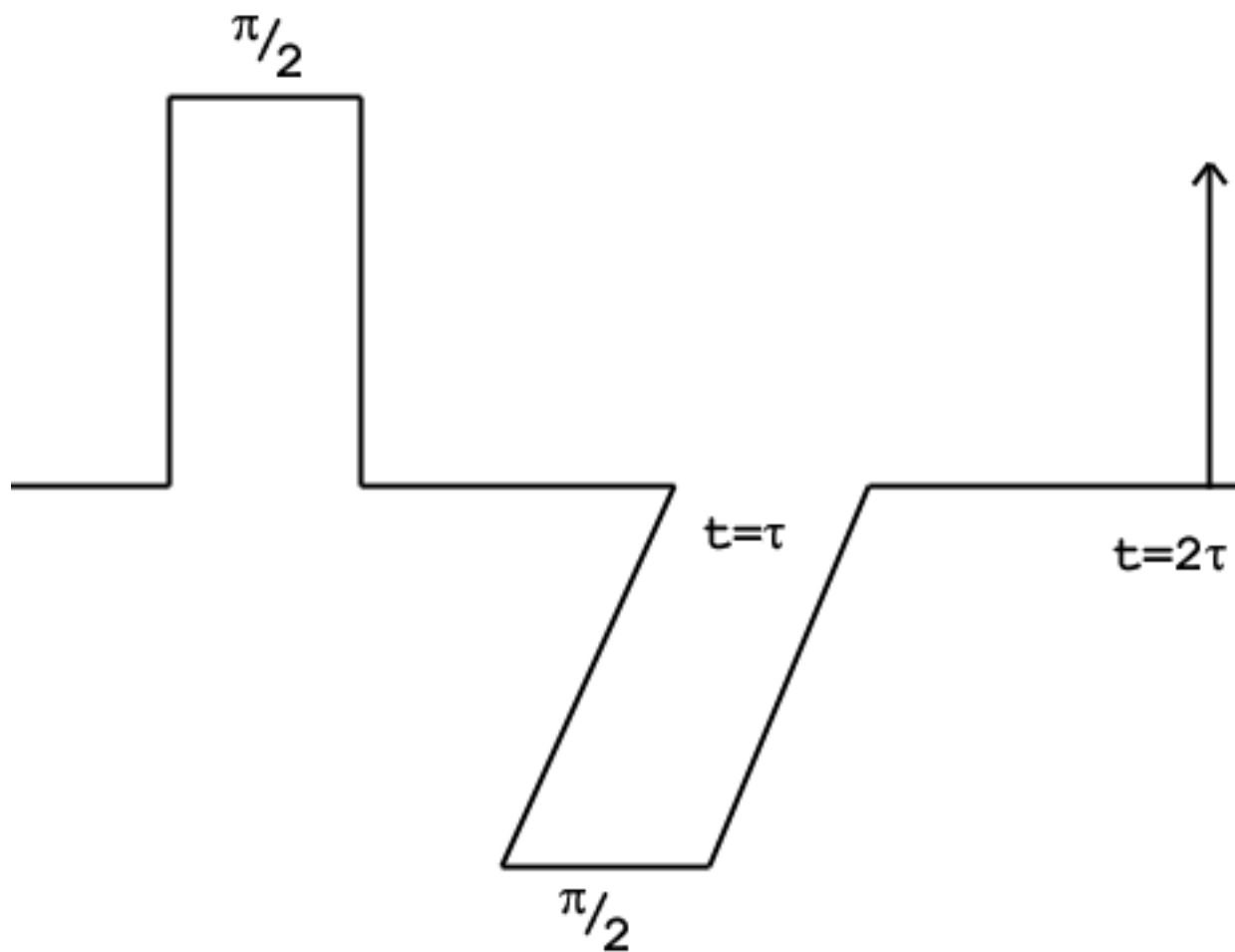


Figure 2.5: Quadrupolar echo pulse sequence with initial  ${}^{90^0}_{0^0}$  pulse at  $t = 0$  and a  ${}^{90^0}_{90^0}$  pulse at  $t = \tau$  which causes a refocussing of the magnetization at  $t = 2\tau$  resulting in a spin echo.

spectroscopy measure directly the bulk phase of the sample and, by using the lever rule, the concentration of lipids in each of the two phases can be determined. Since the total phase of the sample is being used and phase separation is being measured directly, slight inhomogeneities have much less effect.

When a sample composed of a mixture of two lipids is placed at a temperature between the transition temperatures of the two individual lipid components, the sample then enters a two phase region where a fraction of the lipids is in the gel phase and a fraction of the lipids is in the liquid crystalline phase.

An isothermal line, or tie line, drawn across the phase diagram in this two-phase region will intersect the solidus and liquidus boundaries at two points called endpoints (see Figure 2.6). If the sample has a composition  $x_i$  (composition referring to the mole fraction of DSPC) the sample can be separated into its two endpoints, denoted by  $x_g$  for the gel endpoint and  $x_f$  for the liquid crystalline endpoint, which are determined by the tie line for the given temperature. The fraction of the sample which is in the liquid crystalline phase for that temperature is then given by the lever rule

$$a_i(T) = \frac{[x_i - x_g(T)]}{[x_f(T) - x_g(T)]} \quad (2.16)$$

and the fraction of the sample in the gel phase is  $1 - a_i(T)$ . The actual amount of DMPC in the fluid phase is given by

$$f_i = a_i \frac{(1 - x_f)}{(1 - x_i)} \quad (2.17)$$

where  $1 - x_g$  and  $1 - x_i$  are the phospholipid concentrations of the liquid crystalline phase domain and the sample, respectively.

If we assume that the exchange of lipids between the two phases is fairly slow compared to the  $^2\text{H}$  NMR time scale, then within the two phase region, the resultant spectrum for a particular sample is composed of the superposition of the endpoint spectra associated

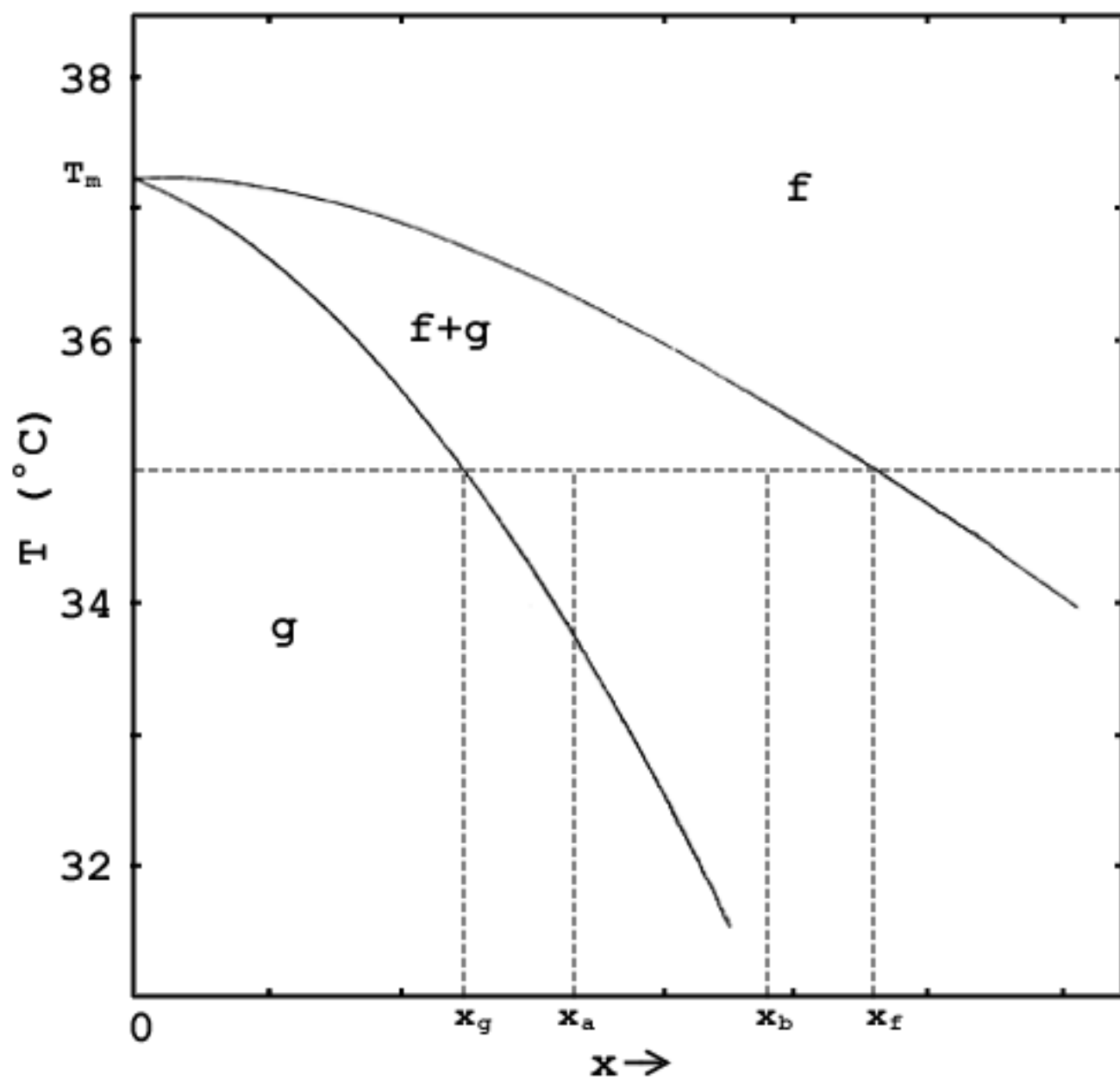


Figure 2.6: A possible phase diagram for a liquid crystalline to gel phase transition with the endpoint concentrations,  $x_g$  and  $x_f$  determined by an isothermal line drawn through the sample concentration  $x_a$  or  $x_b$ .

with the given temperature. If we take two samples at a temperature  $T$  with compositions  $x_a$  and  $x_b$  then the spectrum of the first sample is given by

$$S(x_a, T) = f_a S_f(x_f, T) + (1 - f_a) S_g(x_g, T) \quad (2.18)$$

while for the second sample

$$S(x_b, T) = f_b S_f(x_f, T) + (1 - f_b) S_g(x_g, T) \quad (2.19)$$

where  $S_f(x_f, T)$  and  $S_g(x_g, T)$  are the endpoint spectra associated with the liquid crystalline phase at endpoint concentration  $x_f$  and the gel phase at endpoint concentration  $x_g$ . Therefore, if two spectra are taken from two samples with different compositions but at the same temperature within the two phase region, both spectra are composed from the same liquid crystalline and gel endpoints.

By solving the previous two equations for each of the endpoint spectra we get

$$S_g(x_g, T) = \frac{1}{(f_b - f_a)} [f_b S(x_a, T) - f_a S(x_b, T)] \quad (2.20)$$

and

$$S_f(x_f, T) = \frac{1}{(f_a - f_b)} [(1 - f_b) S(x_a, T) - (1 - f_a) S(x_b, T)] \quad (2.21)$$

From this, we have shown that each of the endpoint spectra can be obtained by subtracting a certain amount of one sample spectrum from another providing both spectra are at the same temperature and that all spectra have been normalized to unit area.

If we let  $x_b$  correspond to the concentration of the sample with the higher liquid crystalline phase content, then it should be possible to subtract a fraction  $K$  of  $S(x_b, T)$  from  $S(x_a, T)$  so that the resulting spectrum has only gel endpoint characteristics (see Figure 5.3). This value of  $K$  is given by

$$K = \frac{a_a(1 - x_b)}{a_b(1 - x_a)} \quad (2.22)$$

Similarly, it should be possible to subtract a fraction  $K'$  of  $S(x_a, T)$  from  $S(x_b, T)$  to obtain a spectrum that has only the characteristics of a liquid crystalline endpoint spectrum (see Figure 5.4). This value of  $K'$  can be obtained from

$$K' = \frac{(1 - a_b)(1 - x_a)}{(1 - a_a)(1 - x_b)} \quad (2.23)$$

In the end, this gives us equations for the gel and liquid crystalline endpoint concentrations

$$x_g = \frac{[(1 - x_b)x_a - K(1 - x_a)x_b]}{[(1 - x_b) - K(1 - x_a)]} \quad (2.24)$$

and

$$x_f = \frac{[(1 - x_a)x_b - K'(1 - x_b)x_a]}{[(1 - x_a) - K'(1 - x_b)]} \quad (2.25)$$

These concentrations can then be plotted to give the phase diagram of the lipid mixture with the  $x_g$  values corresponding to the solidus boundary and the  $x_f$  values corresponding to the liquidus boundary.

## Chapter 3

### Lipids and Lipid Bilayers

#### 3.1 Lipid Structure

A lipid has two main regions in its structure. There is a polar headgroup which usually contains a negatively charged phosphate ion that makes this region very hydrophilic. The other region is hydrophobic since it is composed of two long hydrocarbon chains.

This dual nature within the lipid molecules means that when lipids are placed in water, they tend to form a bilayer with the hydrophobic carbon chains hidden on the inside protected by the polar headgroups facing out towards the water.

The two molecules being studied, i.e. DMPC and DSPC, differ in the length of their hydrocarbon chains by four carbons. DMPC has fourteen carbons along each of its hydrocarbon chains and DSPC has eighteen carbons along each of its hydrocarbon chains.

#### 3.2 Lipid Phases

The study of the phase behaviour of lipids is one method that is useful in helping understand how the structure affects the lipid bilayers. A lipid has two phases that take it from the gel phase, a very ordered state, to the liquid crystalline phase, a very disordered state.

The gel phase is characteristic of low temperatures, where the lipid molecules do not show much lateral motion and all the hydrocarbon chains are in the trans conformation leading to a very closely packed structure. As the temperature is raised, the lipids move

into the liquid crystalline phase where some carbons on the hydrocarbon chains switch to the *cis* conformation which lead to kinks, causing the bilayer to lose its tightly packed structure and become more fluid. The rate of lateral diffusion of the lipids increases by two orders of magnitude when it goes from a low to a high temperature (10).

Each lipid has its own characteristic transition temperature which depends on the length of the lipid's hydrocarbon chains, the net charge on the lipid, the chemical environment of the lipid and the presence of cholesterol in the lipid bilayer.

Since the two lipids being used in this experiment only differ in the length of their hydrocarbon chains, this should be the only factor that determines the transition temperature. In general, the longer the hydrocarbon chain, the lower the transition temperature from the gel to the liquid crystalline phase. Therefore, the DSPC should be the first to change from gel into fluid in the samples.

### 3.3 Deuterium NMR

It would seem that protons should be the ideal choice for the nuclei to be studied in the lipid bilayers because of their abundance and large magnetic moment but it turns out that deuterons are the preferred nuclei. The deuteron has an electric quadrupole moment which is small enough that the quadrupole interaction can simply be treated as a first order perturbation on the Zeeman interaction. Also, the quadrupolar moment is small enough that solid state NMR techniques can be used.

Most of the useful interactions between nuclei have values much less than the Larmor frequency in a typical magnetic field. For example, in a magnetic field of 8.5T, the deuteron Larmor frequency is about 55MHz and the maximum quadrupolar splitting for an  $^2\text{H}$  in a C- $^2\text{H}$  bond is only 252kHz. Also, the  $^2\text{H}$ - $^2\text{H}$  dipolar splitting is around a few kHz, the  $^2\text{H}$ - $^1\text{H}$  dipolar splitting is of the order of 10kHz and the chemical shift dispersion

is only about 1kHz. Therefore, it is possible to neglect the dipolar interactions and chemical shift dispersion and take the deuteron as an isolated nucleus using first order perturbation theory to treat the quadrupolar interactions. This gives a much simpler analysis of the model.

Another problem with protons is that a line broadening is produced by the dipolar interactions between protons and this broadening has about the same value as the line splitting due to neighbouring dipolar interactions among protons on the chains. This results in a single broad absorption peak from which the details of individual protons at different positions along the hydrocarbon chains are hard to obtain.

on the other hand, the quadrupolar interaction between deuterons on the chain is much higher in value than the line splitting produced by dipolar interactions between neighbouring deuterons. Therefore, each individual position along the hydrocarbon chain can be resolved. Deuterons also do not affect significantly the dynamics of the lipid bilayer and therefore can be used to replace protons along the hydrocarbon chains without any great effect to the system (9).

The types of membranes being studied are known as partially ordered systems. Their molecular motions tend to be anisotropic which cause the motional averaging of the orientation dependent interactions to be incomplete. This extra part which is not averaged away can be used to determine the symmetry of the system and of the molecular motions, the amplitude and rate of the motions and the occurrence of any phase transitions.

## Chapter 4

### Experimental Set-up

#### 4.1 Sample Preparation

The samples used in this experiment were mixtures of DMPC and DSPC. Since the technique being used to study the samples was  $^2\text{H}$  NMR difference spectroscopy, one of the samples needed to be deuterated to produce a deuterium signal and the DMPC lipid was chosen in this case. Each DMPC lipid was deuterated along its hydrocarbon chains to obtain  $\text{DMPC}_{\text{d}54}$ . The lipids were purchased from Sigma (Sigma-Aldrich Corp., St. Louis, MO, U.S.A.).

To ensure that a good signal was produced for the NMR spectrometer, 40mg of DMPC was always present in each sample and the amount of DSPC varied depending on the concentration wanted for the study. The mole fractions of DSPC actually used in the experiment were 0, 0.252, 0.351, 0.403, 0.501, 0.504, 0.603 and 0.703.

A stock solution for each of the two lipids was made by dissolving the lipids in methanol and therefore the samples were prepared by measuring volumetrically known amounts of the stock solutions. The solvent was then removed using rotary evaporation and also by pumping the sample overnight in a dessicator.

The sample was then scraped into an 8mm glass NMR tube and about  $350\mu\text{L}$  of 50mM phosphate buffer of pH 7 was added to hydrate the sample. The tube was then sealed with a teflon cap and also some teflon tape to prevent evaporation. Each sample was checked for lipid degradation by using thin layer chromatography and no signs of

degradation were found.

## 4.2 NMR Spectrometer

The NMR spectrometer used in the experiment was 'homebuilt' with the general set-up shown in Fig. 4.1 (11). The experiment was conducted at 23MHz, the resonant frequency of deuterons in the super conducting magnet.

A Nicolet 2090 digital oscilloscope was used to digitize the signal and a Tandy 1200 microcomputer was used to accumulate and average the signal.

The temperature of the sample was controlled by another microcomputer which was hooked up to a copper oven surrounding the sample area.

The Tandy 1200 also controlled the pulse programmer which would open and close gates to create the correct pulse sequence. The actual rf was produced by the frequency synthesizer with a frequency of 23.215MHz. This base frequency was split so that part of it acted as a reference and the other part went through a 30W amplifier and a high power transmitter to the probe containing the sample.

The probe consists of a coil, with an inductance of about  $1\mu\text{H}$ , surrounding the sample which is placed inside a superconducting magnet. The crossed diodes allow the transmitter to be connected to the probe or receiver selectively. The crossed diodes associated with the receiver are placed at a distance  $\lambda/4$  from the probe circuit in order to isolate the transmitter from the receiver. When there is high power going through the transmitter, the crossed diodes are turned on and no power goes to the receiver. Following the pulse, the diodes are turned off and the receiver is ready to receive the much lower power signal from the probe. The variable capacitors are used to tune the probe circuit to the Larmor frequency which is needed in order to produce a signal from the sample.

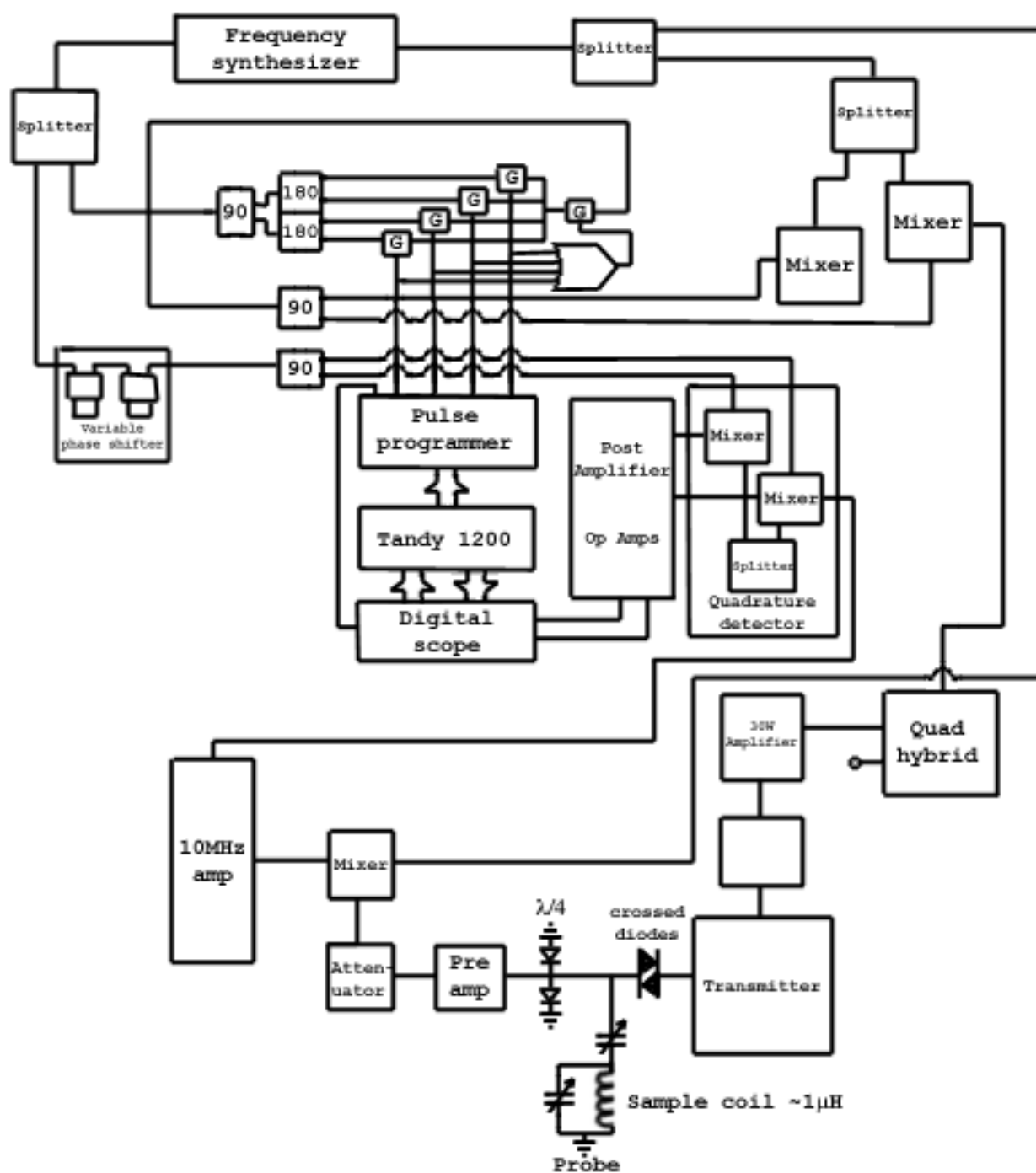


Figure 4.1: Schematic diagram for the NMR spectrometer.

This signal then goes to the preamp and gets mixed with the original rf source. The signal is amplified in the 10MHz range and detected by the quadrature detector which finds the  $0^0$  and  $90^0$  shifted signals. This final signal is amplified and digitized using the oscilloscope.

### 4.3 Measurement of Quadrupole Echo

The Fourier transform was begun at the top of the echo which eliminated any dead time problems. To improve the signal to noise ratio, odd and even points were treated separately to obtain two different free induction decay curves (one using the odd points and one using the even points). In each set, the points were shifted either up or down the curve so that the two free induction decays had points at the peak of their echo. These two fids were added to obtain a modified free induction decay.

The signals were accumulated with dwell times of  $2\mu\text{s}$  in the gel phase and  $4\mu\text{s}$  in the liquid crystalline phase. The  $90^0$  pulse length ranged between 6 and  $8\mu\text{s}$  and the spacing between the two pulses was  $35\mu\text{s}$ . For each spectrum, 4000 transients were collected and averaged to give the final results.

## Chapter 5

### Results and Discussion

#### 5.1 Gel and Liquid Crystalline Spectra

The reason that deuterium NMR can be used to determine the phase diagram for lipid mixtures is that the gel and liquid crystalline spectra are very different from one another.

The liquid crystalline spectrum has large central peaks and sharply defined edges. The peaks are due to the methyl groups at the end of each hydrocarbon which are free to rotate since there is no steric hindrance from other chains (see Figure 5.1a). The 90° edges show a well-defined order parameter plateau defined by the order parameter of the C-<sup>2</sup>H bond vector. This spectral shape can be simulated by a superposition of  $I = 1$  quadrupolar powder patterns.

The gel spectrum is much broader than the liquid crystalline spectrum and the 90° edges have disappeared (see Figure 5.1b). The spectrum is much more rounded with most of the intensity out in the wings.

#### 5.2 The Determination of the Endpoint Concentrations

The sample is studied as a function of temperature. Therefore, the spectra go through an observable change as the transition temperature is reached (see Figure 5.2). When the sample is in the two-phase region, the spectra have a mixture of the gel and liquid crystalline characteristics.

The actual process used to determine the endpoint concentrations is to take pairs of

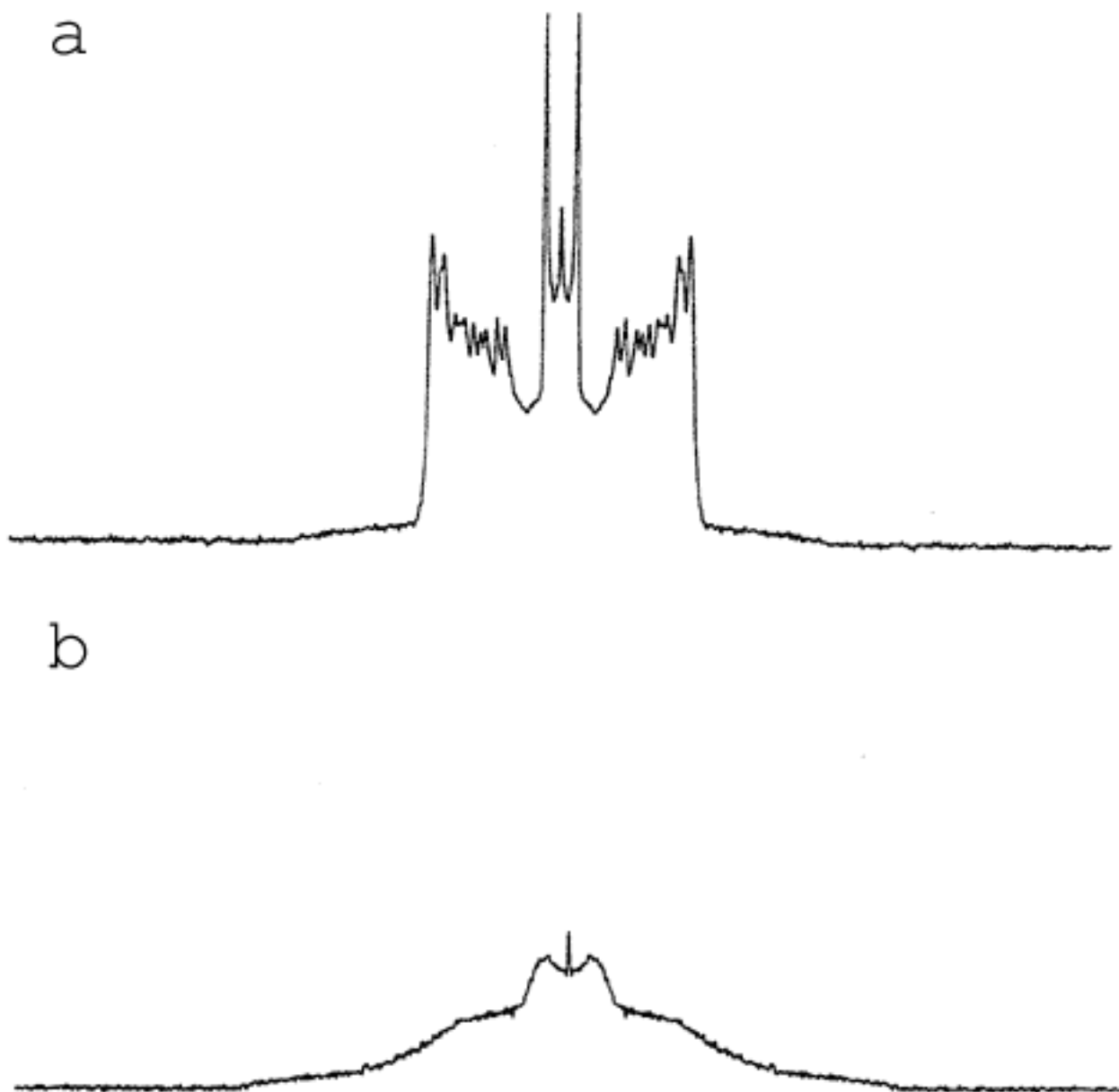


Figure 5.1: The characteristic spectra of: a) a sample liquid crystalline phase and b) a sample in the gel phase.

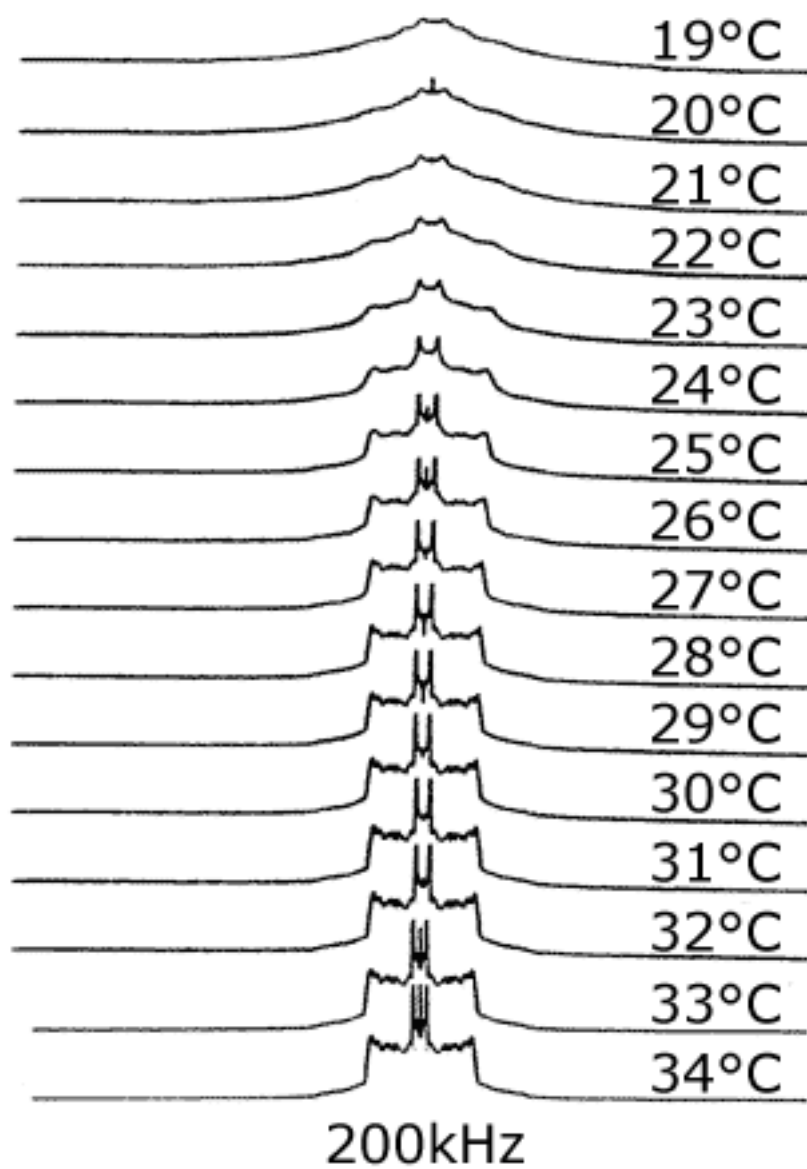


Figure 5.2: The temperature dependence of the spectra of a sample with concentration 0.603. The sample goes through a noticeable phase transition at around 27°C–21°C.

spectra which are at the same temperature and subtract them to obtain spectra that have the characteristic endpoint lineshape.

To determine  $x_g$ , a fraction,  $K$ , of the spectrum of the sample with the lower DSPC concentration is subtracted from the sample with the higher DSPC concentration so that the resulting spectrum has the characteristic gel shape (see Fig 5.3). From the value of  $K$  and the concentrations of each of the samples being subtracted, the endpoint concentration,  $x_g$ , can be determined by using equation (2.24).

There is actually a range of  $K$  values for which the resulting spectrum has the characteristic gel shape. This range is determined by the value of  $K$  that produces a spectrum which has just lost its  $90^0$  edges and the value  $K$  which causes the spectrum to show dips on its rounded shoulders. The average value of  $K$  is then calculated and used to determine  $x_g$ .

The determination of  $x_f$  was done in a similar fashion by finding  $K'$ . This was done by subtracting a fraction  $K'$  of the higher DSPC concentration spectrum from the lower one until a liquid crystalline spectrum was observed (see Figure 5.4).

As before, a range of  $K'$  values was found. The liquid crystalline spectrum only has intensity in a narrow range so that any deviation of the spectrum from the baseline beyond the  $90^0$  shoulders would indicate the presence of a gel component. Therefore the range of  $K'$  values was determined from the value of  $K'$  at which the spectrum had intensity which was above the baseline beyond the  $90^0$  shoulders to the value of  $K'$  where the spectrum had intensity below the baseline beyond the  $90^0$  shoulders. The average value of  $K'$  was then determined and substituted into equation (2.25) to find  $x_f$ .

For each temperature, there is a large number of pairs that can be used to determine the values of  $x_g$  and  $x_f$ . Unfortunately, not all subtractions produce spectra that have the correct lineshape and therefore they can not all be used. When all the subtractions for a given temperature are performed, an associated error with the result has to be

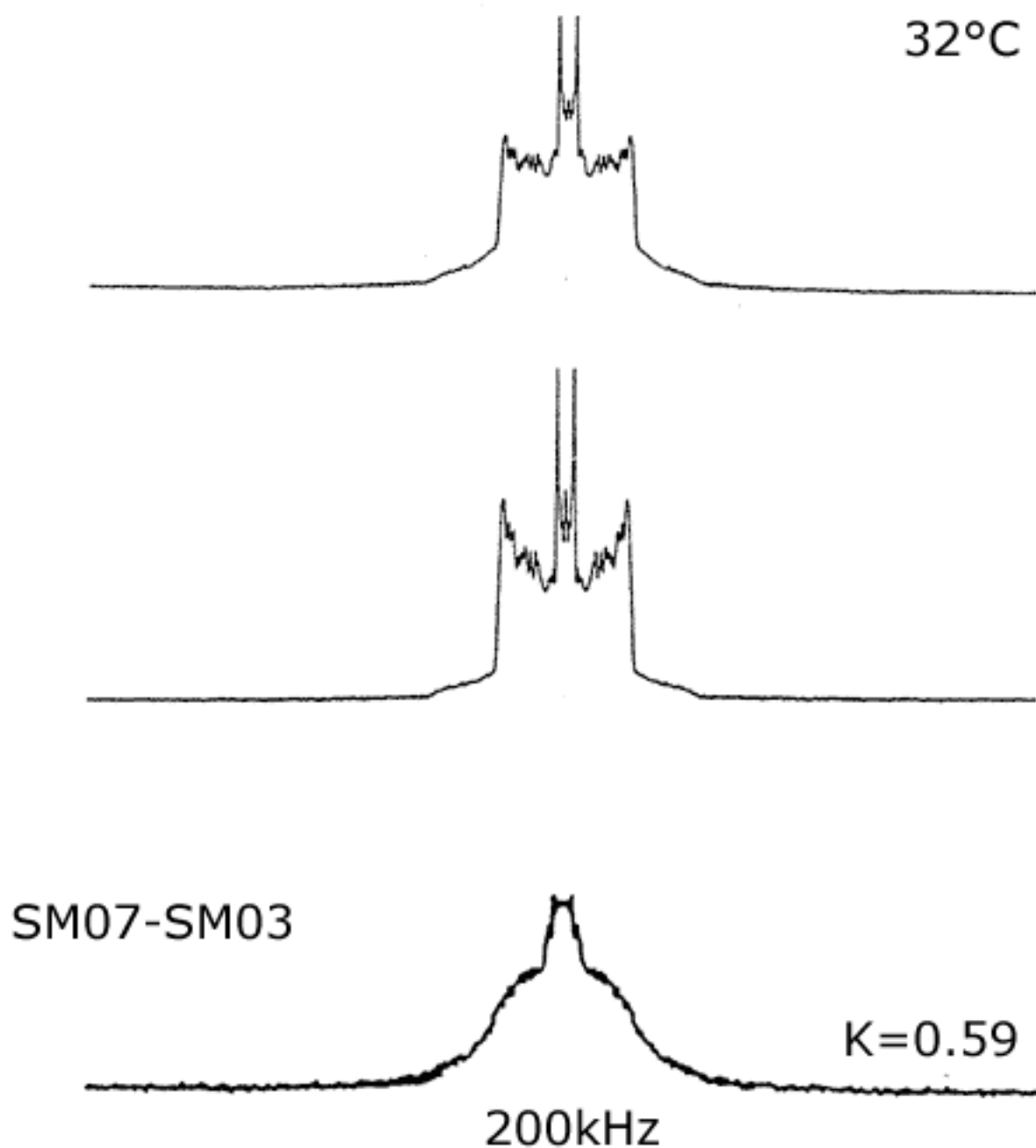


Figure 5.3: A spectral subtraction, between samples with concentration 0.603 and 0.351 to obtain a characteristic gel endpoint spectrum with  $K = 0.59$  at  $32^{\circ}\text{C}$ . This gives  $x_g = 0.731$ .

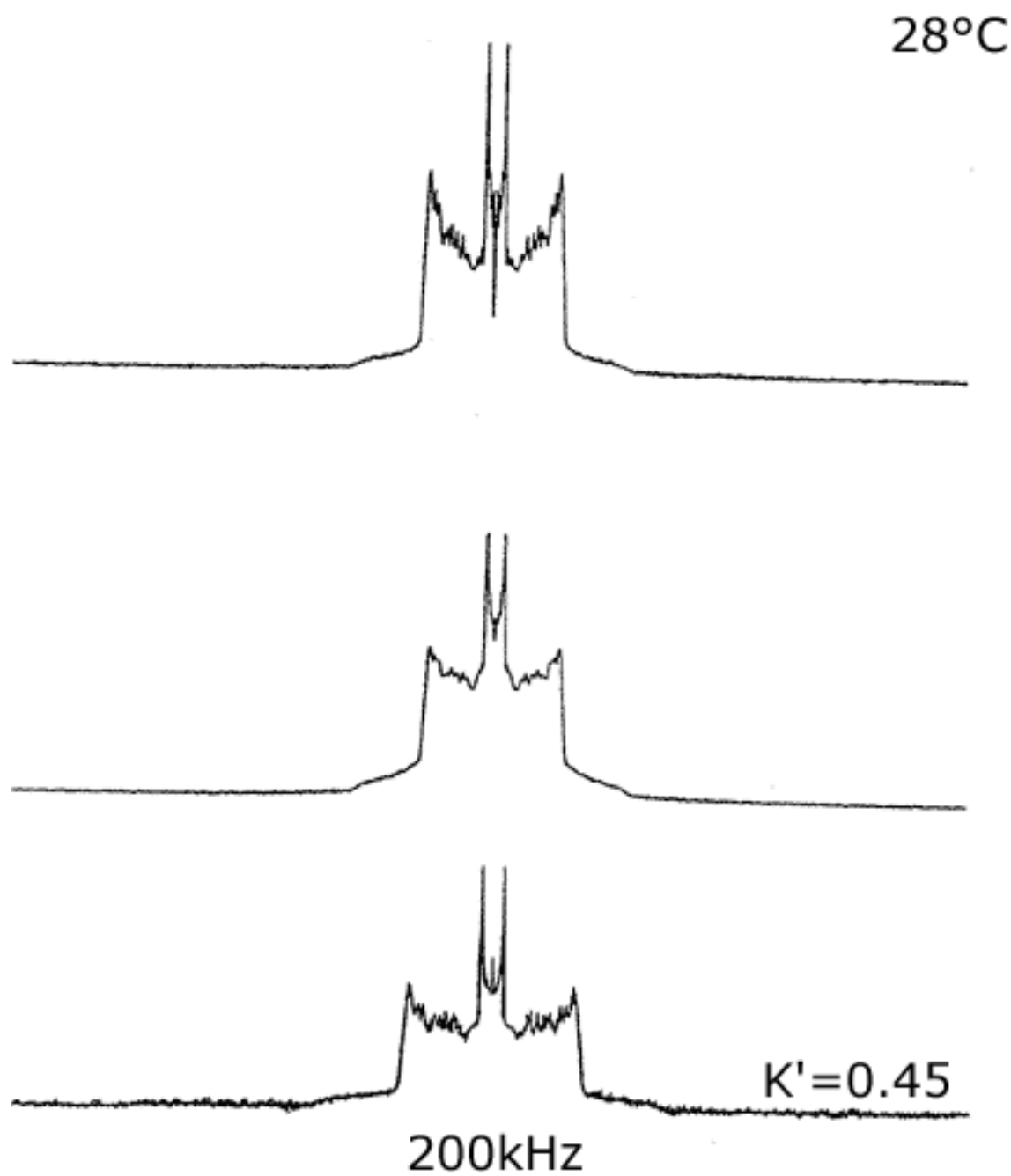


Figure 5.4: A spectral subtraction, between samples with concentration 0.252 and 0.403, to obtain the characteristic liquid crystalline endpoint spectrum with  $K' = 0.45$  at  $28^{\circ}\text{C}$ . This gives  $x_f = 0.045$ .

determined so that, in the end, a weighted mean can be found.

One problem that may occur when the method of  $^2\text{H}$  NMR difference spectroscopy is used is that during the time between pulses, about  $70\mu\text{s}$ , the sample may undergo transverse relaxation. If this relaxation is not the same in both the gel and liquid crystalline phase then the intensities of the respective signals will vary.

Since the intensities, represented by the area under the spectra, are used as a direct measure of the amount of lipid in a given phase, errors could occur when comparing spectra from each of the phases unless the difference in transverse relaxation is taken into account.

The sample in the gel phase has usually decayed by an extra factor  $R$  compared to the sample in the liquid crystalline phase. The value of  $R$  can be found by comparing the intensity of the signal at temperatures just above and below the boundary of the two-phase region, i.e. just before the sample shows gel characteristics and just after the sample has lost all liquid crystalline characteristics.

This intensity is determined by the area under the spectrum and is proportional to the number of deuterons resonating at the indicated frequency. To find this intensity, we can calculate  $M_0$  which refers to the zeroth moment of the spectrum. The moments of the spectrum can be found by

$$M_n = 1/A \int \omega^n f(\omega) d\omega \quad (5.1)$$

where  $A = \int f(\omega) d\omega$ .

A ratio between the zeroth moment of the liquid crystalline spectrum at the liquidus boundary and the zeroth moment of the gel spectrum at the solidus boundary can be used to determine the loss in intensity due to transverse relaxation. This ratio is actually the value for  $R$ .

Two values of  $R$  were calculated for each different sample concentration. The average

mole fraction of DSPC	temperatures	intensity of signal ( $M_0 \times 10^{11}$ )	$R$ $M_0$ of gel $M_0$ of l.c
0.252	35 <sup>0</sup> / 16 <sup>0</sup>	4.756 / 6.985	0.734
0.252	36 <sup>0</sup> / 15 <sup>0</sup>	4.718 / 7.218	0.765
0.351	42 <sup>0</sup> / 16 <sup>0</sup>	6.264 / 8.918	0.712
0.351	44 <sup>0</sup> / 14 <sup>0</sup>	6.270 / 8.959	0.714
0.403	42 <sup>0</sup> / 15 <sup>0</sup>	5.559 / 9.036	0.813
0.403	44 <sup>0</sup> / 14 <sup>0</sup>	5.579 / 9,086	0.814
0.504	43 <sup>0</sup> / 15 <sup>0</sup>	4.586 / 6.921	0.755
0.504	45 <sup>0</sup> / 14 <sup>0</sup>	4.586 / 6.908	0.753
0.603	49 <sup>0</sup> / 17 <sup>0</sup>	5.367 / 8.718	0.812
0.603	51 <sup>0</sup> / 16 <sup>0</sup>	5.364 / 8.573	0.799
0.703	49 <sup>0</sup> / 17 <sup>0</sup>	5.498 / 9.233	0.840
0.703	51 <sup>0</sup> / 16 <sup>0</sup>	5.587 / 9.225	0.826

Table 5.1: Determination of  $R$  values

value of  $R$  was calculated as 0.778 and the values used to determine  $R$  are found in Table 5.1.

The  $R$  value can be used to modify equations (2.24) and (2.25) if  $K$  is replaced by  $KC$  and  $K'$  is replaced by  $K'/C$  where

$$C = \frac{1 + f_a((1 - R)/R)}{1 + f_b((1 - R)/R)} \quad (5.2)$$

The phase boundaries,  $x_g$  and  $x_f$ , were first determined with  $R = 1$  and then their values were used to calculate  $C$ . This value of  $C$  could then be used to modify the previous endpoint concentrations so that the problem with the difference in transverse relaxation could be fixed.

One of the errors associated with this experiment is the uncertainty in the values of  $x_a$  and  $x_b$ . Since each sample was measured volumetrically, there is a small uncertainty in the volume of each lipid mixed together. This error was taken to be  $\Delta V/V = 0.03$ .

We know that the liquid crystalline endpoint concentration is given by

$$x_f = \frac{[(1-x_a)x_b - K'(1-x_b)x_a]}{[(1-x_a) - K'(1-x_b)]} \quad (5.3)$$

The change in  $x_f$  is given by

$$\Delta x_f^2 = \left(\frac{dx_f}{dx_a}\right)^2 \Delta x_a^2 + \left(\frac{dx_f}{dx_b}\right)^2 \Delta x_b^2 \quad (5.4)$$

$x_a$  and  $x_b$  are related to  $\frac{\Delta n_s}{n_s}$  and  $\frac{\Delta n_m}{n_m}$  (where  $n_s$  and  $n_m$  are the number of moles of DSPC and DMPC respectively) by the equation

$$\Delta x_i^2 = x_i^2(1-x_i)^2 \left[ \left(\frac{\Delta n_s}{n_s}\right)^2 + \left(\frac{\Delta n_m}{n_m}\right)^2 \right] \quad (5.5)$$

Therefore, we can solve equation (5.4) by differentiating equation (5.3) with respect to  $x_a$  and  $x_b$  and substituting their values into the equation.

Differentiation gives us

$$\frac{dx_f}{dx_a} = \frac{-K'(1-x_b)^2(1-K')}{[(1-x_a) - K'(1-x_b)]^2} \quad (5.6)$$

and

$$\frac{dx_f}{dx_b} = \frac{(1-x_a)^2(1-K')}{[(1-x_a) - K'(1-x_b)]^2} \quad (5.7)$$

This will then lead to

$$\Delta x_f^2 = \frac{(1-K')^2(1-x_b)^2(1-x_a)^2 [K'^2(1-x_b)^2 x_a^2 + x_b^2(1-x_a)^2]}{[(1-x_a) - K'(1-x_b)]^4} 2 \left(\frac{\Delta n}{n}\right)^2$$

and

$$\Delta x_g^2 = \frac{(1-K)^2(1-x_b)^2(1-x_a)^2 [(1-x_b)^2 x_a^2 + K^2 x_b^2(1-x_a)^2]}{[(1-x_b) - K(1-x_a)]^4} 2 \left(\frac{\Delta n}{n}\right)^2$$

where we assume that

$$\Delta n_{sa}/n_{sa} = \Delta n_{ma}/n_{ma} = \Delta n_{sb}/n_{sb} = \Delta n_{mb}/n_{mb} = \Delta n/n = \Delta V/V$$

with the subscripts  $a$  and  $b$  referring to samples with concentration  $x_a$  and  $x_b$ .

When evaluating these errors, the endpoint concentrations most affected are those where the subtracted samples are close in concentration and whose concentrations are on the opposite side to the endpoint being determined.

The other error when determining the endpoint concentration is due to the fact that there is a range of  $K$  and  $K'$  values for each subtraction. In this case, the difference between the largest value of  $K$  or  $K'$  in the range and the average value of  $K$  or  $K'$  was squared and added to the previous error due to uncertainty in the concentrations of  $x_a$  and  $x_b$ . This provided an overall error which was used to determine the weighted mean for  $x_f$  and  $x_g$ . The uncertainty in this weighted mean at a given temperature was found by adding together all the inverses of the error for each subtraction and then taking the square root and inverse of this quantity.

The values obtained for  $x_g$  and  $x_f$  are shown in Table 5.2. These were found with  $R = 1$ . Table 5.3 shows the values that were found by taking the  $R$  and  $C$  value into account.

As can be seen from the tables, most of the values were only modified a small amount when the  $C$  value was taken into account. There were exceptions in certain cases with the liquid crystalline endpoints. In some of these liquid crystalline cases, the inclusion of the  $C$  factor caused the value of  $x_f$  to become larger than 1 or smaller than 0 which is obviously not possible. Therefore these values had to be neglected and the average for  $x_f$  changed.

This occurred mainly for  $x_f$  values which, when they were calculated using  $R = 1$ , were found to be very small ( $< .1$ ). Since the use of  $R = 0.778$  made the endpoint concentrations lower, it caused the small values of  $x_f$  to become negative. Therefore only a small fraction of the possible subtractions used to determine  $x_f$  were good and the error associated with the liquidus boundary became very large. For some temperatures,

temperature ( $^{\circ}\text{C}$ )	$x_g$	$\sigma x_g$	$x_f$	$\sigma x_f$
15	-	-	0.247	0.026
16	-	-	0.208	0.019
17	-	-	0.233	0.007
18	-	-	0.179	0.056
19	-	-	0.200	0.029
20	0.692	0.016	0.190	0.018
21	0.660	0.005	0.061	0.037
22	0.637	0.006	0.134	0.029
23	0.658	0.006	0.084	0.064
24	0.676	0.005	0.089	0.048
25	0.702	0.004	0.078	0.028
26	0.742	0.004	0.091	0.036
27	0.769	0.004	0.086	0.024
28	0.763	0.005	0.095	0.024
29	0.767	0.004	0.113	0.017
30	0.776	0.004	0.153	0.018
31	0.775	0.005	0.165	0.013
32	0.776	0.005	0.176	0.012
33	0.778	0.007	-	-
34	0.788	0.012	-	-
35	0.778	0.011	-	-
36	0.792	0.013	-	-

Table 5.2: Endpoint concentrations using  $R = 1$ .

temperature ( $^{\circ}\text{C}$ )	$x_g$	$\sigma x_g$	$x_f$	$\sigma x_f$
20	0.686	0.004	0.218	0.009
21	0.681	0.004	0.157	0.019
22	0.653	0.005	0.149	0.027
23	0.659	0.005	0.255	0.033
24	0.671	0.005	0.175	0.044
25	0.694	0.004	0.159	0.025
26	0.727	0.004	0.152	0.041
27	0.754	0.003	0.105	0.018
28	0.745	0.004	0.082	0.026
29	0.756	0.004	0.096	0.018
30	0.758	0.003	0.152	0.019
31	0.764	0.005	0.158	0.014
32	0.759	0.004	0.170	0.012

Table 5.3: Endpoint concentrations using  $R = 0.778$ .

there were not enough usable subtractions to permit a value of  $x_f$  to be determined. This occurred mostly at the lower temperatures when each sample contained a very large gel phase component and only a very small liquid crystalline phase component.

Since DMPC has a shorter hydrocarbon chain length, it would be expected to go through the liquid crystalline to gel phase transition at a higher temperature than DSPC. Consequently, at low temperatures, most of the liquid crystalline phase was composed of undeuterated DSPC. Therefore, it could not be measured directly using  $^2\text{H}$  NMR. When the two spectra with little liquid crystalline signal were then subtracted to obtain a liquid crystalline endpoint spectrum, the resulting spectrum had a very low signal to noise ratio.

concentration	gel temperature	liquid crystalline temperature
0.252	20 <sup>0</sup> C	33 <sup>0</sup> C
0.351	19 <sup>0</sup> C	35 <sup>0</sup> C
0.403	19 <sup>0</sup> C	36 <sup>0</sup> C
0.504	21 <sup>0</sup> C	40 <sup>0</sup> C
0.603	21 <sup>0</sup> C	43 <sup>0</sup> C
0.703	21 <sup>0</sup> C	45 <sup>0</sup> C

Table 5.4: Temperatures for phase boundaries determined by the sample spectra

### 5.3 The Phase Diagram for DMPC/DSPC

With the values calculated In Table 5.3, the phase diagram for the mixture of DMPC and DSPC can be plotted (see Fig 5.5). The horizontal error bars were determined using the procedure mentioned above.

The points on the liquidus line with the vertical error were determined from the temperature at which the spectrum, as the sample was cooled, first showed signs of a gel component, i.e. the first sign of intensity beyond the 90<sup>0</sup> edges of the liquid crystalline spectrum.

The points on the solidus line with vertical error bars were found from the temperature at which the spectrum, as the sample was cooled, no longer showed any signs of a liquid crystalline component, i.e. the temperature at which there were no longer any signs of 90<sup>0</sup> edges in the spectrum. These values are shown in Table 5.4. The error associated with these temperatures was taken to be  $\pm 0.5^{\circ}\text{C}$  since spectra were obtained at 1<sup>0</sup>C intervals while in the two-phase region.

Around the temperature of 20<sup>0</sup>C, there appears to be a nearly horizontal or isothermal line. This would support the theory of gel immiscibility at low temperatures based on gel immiscibility models for peritectic behavior between gel phases. Therefore, just below

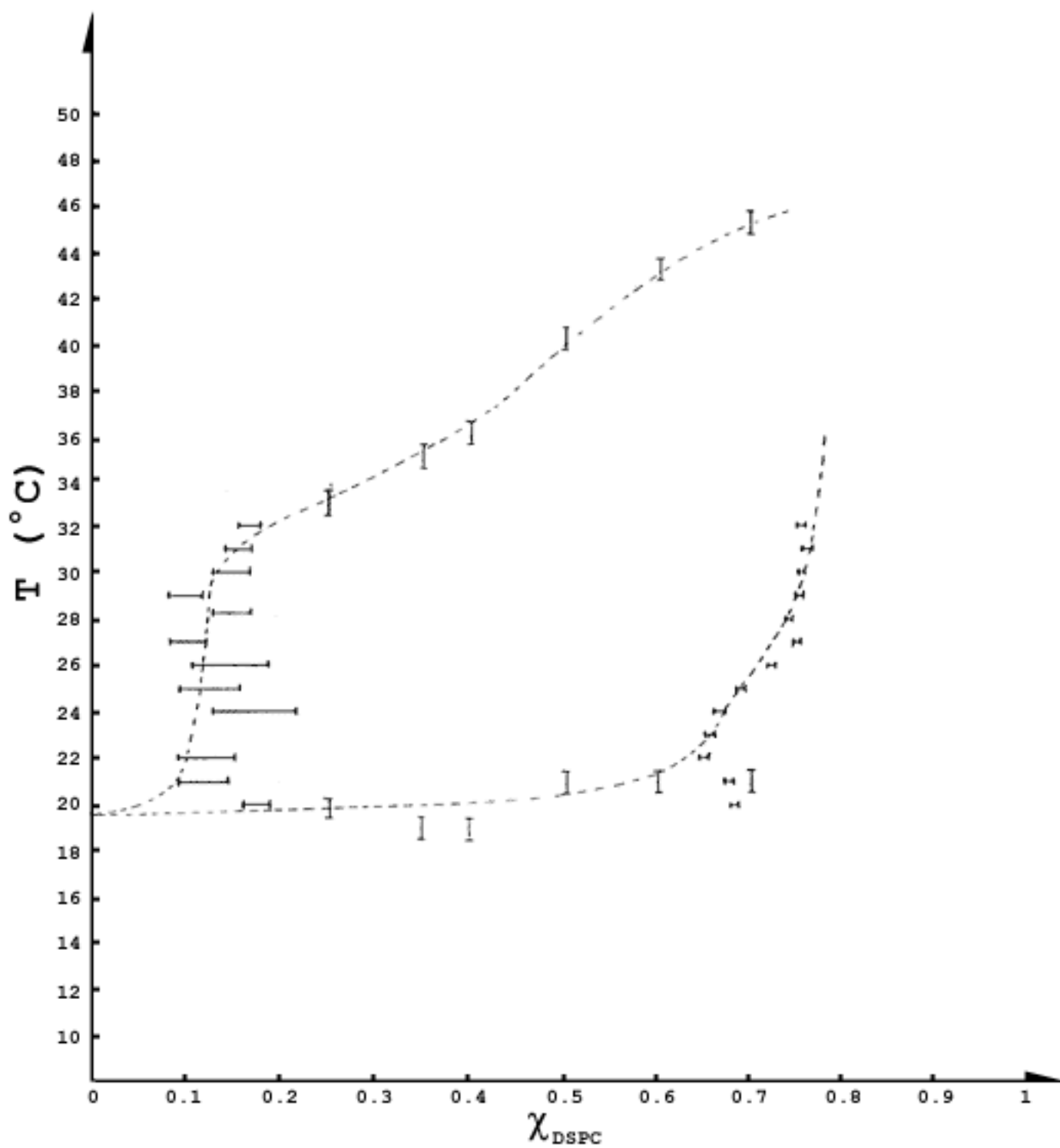


Figure 5.5: The phase diagram obtained for a mixture of DMPC/DSPC

the isothermal line, a mixing of the gel phases is expected to produce a two gel phase region.

There has been support for this model from studies using various other techniques to determine the phase diagram of DMPC and DSPC used in the past (6,12-15) but there has also been support for the gel miscibility theory at low temperature (3,5,16).

This experiment has already been done with  $^2\text{H}$  NMR difference spectroscopy except that in the samples, DSPC was deuterated to yield DSPC<sub>d70</sub> (unpublished). In principle, the phase diagram for the mixture of DMPC and DSPC should be the same in both cases. This turned out not to be the case at all. In the case of deuterated DSPC, the phase diagram showed no signs of an isothermal line and therefore gel miscibility at low temperatures appeared to be present in these samples. It was clearly shown that there was no peritectic behavior possible and therefore it was concluded that gel immiscibility was occurring.

This raises the question as to whether deuteration affects the sample in some way. Some experiments (17-19) seem to suggest that for mixtures of lipids with each component having a pure lipid transition temperature differing by more than  $33^\circ\text{C}$ , gel immiscibility occurs while for differences less than  $33^\circ\text{C}$ , gel miscibility occurs. The difference in transition temperatures for DMPC/DSPC mixtures is  $31^\circ\text{C}$ ; for DMPC/DSPC<sub>d70</sub>, it is  $27^\circ\text{C}$ , and for DMPC<sub>d54</sub>/DSPC it is  $35^\circ\text{C}$ . This rule was actually found using observations for lipids whose differences in transition temperature were due to structural effects not due to an isotope effect that was observed here.

Results from neutron scattering experiments seem to indicate that it does not matter which lipid is deuterated since the results are the same in each case. Therefore, is still not clear what has caused the discrepancy between the phase diagrams for DMPC/DSPC<sub>d70</sub> and DMPC<sub>d54</sub>/DSPC. Also, the problem of whether or not a mixture of DMPC and DSPC is miscible or immiscible at low temperatures has not been solved and further

studies in this area are required.

## Chapter 6

### Conclusion

The phase diagram for a DMPC/DSPC mixture was found using  $^2\text{H}$  NMR difference spectroscopy. The main area of concern was the gel phase at low temperature and whether or not the lipids in this phase were miscible or immiscible. The presence of an isothermal solidus line would suggest immiscibility.

The technique of  $^2\text{H}$  NMR difference spectroscopy consists of subtracting pairs of spectra, which are at the same temperature, until a characteristic endpoint spectrum is obtained, either a gel or liquid crystalline endpoint. This subtraction can then be used to determine the actual concentration of the endpoint. If these values are plotted, then the phase diagram for the mixture can be obtained.

It was found that there was indeed an isothermal line at approximately  $20^\circ\text{C}$  and therefore it would seem that the gel is not miscible for a mixture of  $\text{DMPC}_{\text{d}54}$  and DSPC. This theory has been supported by a number of other authors (6,11-14).

Unfortunately, there has also been evidence for the gel miscibility theory. One of these is basically the same experiment as this one except that the DSPC was deuterated instead of the DMPC. It was found in this case that no isothermal line existed and therefore the gel phase was miscible at low temperatures.

The controversy over whether or not the gel phase shows miscibility or immiscibility has still not been resolved. More studies using  $^2\text{H}$  NMR difference spectroscopy but other sample concentrations could yield a more reliable phase diagram. Also, other newer techniques could be used to determine the phase diagram and perhaps resolve the

controversy.

## References

1. Huschilt, J. C., Hodges, R. S. and Davis, J. H. (1985) *Biochemistry* 24, p. 1377–1386.
2. Phillips, M. C., Ladbroke, B. D. and Chapman, D. (1970) *Biochim. Biophys. Acta* 196, p. 35–44.
3. Mabrey, S. and Sturtevant, J. M. (1976) *Proc. Natl. Acad. Sci. U.S.A.* 73, p. 3862–3866.
4. Shimshick, E. J. and McConnell, H. M. (1973) *Biochemistry* 12, p. 2351–2360.
5. Wilkinson, D. A. and Nagle, J. F. (1979) *Biochemistry* 18, p. 4244–4249.
6. Schmidt, G. and Knoll, W. (1986) *Chem. Phys. Lipids* 39, p. 329–339.
7. Cohen-Tannoudji, C., Diu, B. and Laloe, F. *Quantum Mechanics*, vol. 2 (1977), Hermann, Paris.
8. Bloch, F., Hansen, W. W. and Packard, M. (1946) *Phys. Rev.* vol. 70, no. 7, p. 460.
9. Davis, J. H., Jeffrey, K. R., Bloom, M., Valic, M. I. and Higgs, T. P. (1976) *Chem. Phys. Lett.* 42, p. 390–394.
10. Davis, J. H. (1989) *Advances in Magnetic Resonance* 13, p. 195–223.
11. Morrow, M. R. (1990) *Biochim. Biophys. Acta* 1023, p. 197–205.
12. Knoll, W., Ibel, K. and Sackmann, E. (1981) *Biochemistry* 20, p. 6379–6383.

13. Knoll, W., Schmidt, G., Sackmann, E. and Ibel, K. (1983) *J. Chem. Phys.* 79, p. 3439–3443.
14. Quinn, P. J. (1987) *Nat. Prod. Rep.* 4, p. 129–137.
15. Quinn, P. J. (1989) *J. Bioenergetics and Biomembranes* 21, p. 3–19.
16. Mendelsohn, R. and Maisano, J. (1978) *Biochim. Biophys. Acta* 506, p. 192–201.
17. Curatolo, W., Sears, B. and Neuringer, L. J. (1985) *Biochim. Biophys. Acta* 817, p. 261–270.
18. Mason, J. T. (1988) *Biochemistry* 27, p. 4421–4429.
19. Schroeder, F. and Nemezc, G. (1989) *Biochemistry* 28, p. 5992–6000.